A Niclosamide Prodrug SSL-0024 with Enhanced Bioavailability Suppresses Hepatocellular Carcinoma via Multi-Pathway Signaling Inhibition

Mingdian Tan[1, #], Steve Schow[2], Yi Liu[1], Robert Lum[3], Dawiyat Massoudi[4], Renumathy Dhanasekaran[4], Samuel So[1], Mei-Sze Chua[1, #]

1. Department of Surgery, School of Medicine, Asian Liver Center, Stanford, CA 94305, USA
2. Department of Chemical and Systems Biology Operations, Stanford University School of Medicine
3. RTL Consulting Group LLC
4. Division of Gastroenterology and Hepatology, Department of Medicine, Stanford University, CA 94305, USA

Corresponding authors

Mingdian Tan, Ph.D., Research Scientist

Department of Surgery, School of Medicine, Asian Liver Center, 1201 Welch Road, Palo Alto, CA 94305, USA

Email: mdtan@stanford.edu

Mei-Sze Chua, Ph.D., Senior Scientist

Department of Surgery, School of Medicine, Asian Liver Center, 1201 Welch Road, Palo Alto, CA 94305, USA

Email: mchua@stanford.edu

Abstract:

Background:

Hepatocellular carcinoma (HCC) remains a leading cause of cancer-related mortality worldwide, highlighting the urgent need for effective therapies. Niclosamide, an FDA-approved anthelmintic, reverses HCC gene expression profile to that of normal hepatocytes, and exhibits promising anti-tumor activity in HCC *in vitro*; however, its clinical translation is limited by poor aqueous solubility, low bioavailability, and short systemic exposure, resulting in lack of in vivo activity. We previously used an established phosphate prodrug approach to provide proof-of-concept that increasing oral bioavailability was essential for niclosamide to achieve in vivo anti-tumor activity.

Methods:

We designed a panel of novel niclosamide prodrugs and screened eight candidates for water solubility, chemical stability, and in vitro anti-proliferative activity in HCC cell lines. The lead compound, SSL-0024, was further evaluated for its pharmacokinetics and anti-tumor efficacy in immunodeficient mice bearing orthotopic HCC patient-derived xenografts (PDX). Mechanisms underlying its observed activity were assessed through protein-level analysis of AKT–mTOR–STAT3, RAF, Wnt/β-catenin signaling pathways, vasorin-associated pathways, and PD-L1.

Results:

SSL-0024 demonstrated markedly improved aqueous solubility and stability in gastric and plasma conditions, supporting oral administration. Pharmacokinetic analyses revealed a plasma half-life of ~24 hours, dramatically extended relative to native niclosamide. Once daily oral administration of SSL-0024 (100 mg/kg) in orthotopic HCC PDX mice achieved ~60% tumor growth inhibition at only ~46.8% of the dose required for the positive control (niclosamide

ethanolamine), with minimal systemic toxicity. Mechanistically, SSL-0024 concurrently suppressed AKT–mTOR–STAT3 signaling, RAF kinases, Wnt, and VASN-associated pathways, with additional downregulation of PD-L1, resulting in reduced proliferation, survival, and immune-evasion signaling.

Conclusion:

Through rational design and systematic screening, we have identified a lead niclosamide prodrug candidate, SSL-0024, which exhibited improved water solubility and stability, extended plasma half-life, enhanced oral bioavailability, and preservation of biological activity in vitro and in vivo. Future studies will include combination therapy with standard-of-care treatments, as well as safety and formulation studies to enable its clinical translation for the treatment of HCC and other solid tumors impacted by the multiple oncogenic pathways modulated by niclosamide.

Keywords: Hepatocellular carcinoma; Niclosamide Prodrug; Pharmacokinetic optimization; Oncogenic signaling pathways; Sulfate prodrugs

Introduction

Hepatocellular carcinoma (HCC) is the most common type of primary liver cancer, representing approximately 75–90% of cases, ranking among the fifth to sixth most common cancers and remaining the third leading cause of cancer-related mortality worldwide, with over 800,000 deaths annually[1]. Most patients present with advanced disease in the context of chronic liver injury, and despite recent advances in systemic therapy, sustained treatment responses remain limited due to molecular heterogeneity and compensatory activation of parallel oncogenic

pathways[2]. Therapeutic strategies capable of simultaneously suppressing convergent survival networks while maintaining tolerable systemic exposure remain urgently needed.

Niclosamide, an FDA-approved anthelmintic drug, has emerged as a candidate for oncologic repurposing because of its multi-target activity. Mechanistic studies have demonstrated that it suppresses multiple signaling pathways, including but not limited to, Wnt/β-catenin signaling through LRP6 degradation [3], STAT3-dependent transcriptional activity in cancer models[4], and mTOR [5]. Through coordinated interference with survival and proliferation pathways, niclosamide exhibits in vitro anti-tumor effects in HCC[5-7] and other types of cancers [8-13]. However, despite robust preclinical efficacy, clinical translation of niclosamide in solid tumors has been limited by extremely poor aqueous solubility and the resulting low oral bioavailability, as well as rapid systemic clearance [14].

Specifically for HCC, we previously reported that niclosamide effectively reversed HCC gene expression profiles to that of normal hepatocytes, suggesting its anti-HCC potential[5]. However, in vivo activity was only observed with a more water-soluble form, niclosamide ethanolamine (NEN), which is not FDA approved for human use. In an effort to aid clinical translation of niclosamide, we reported a proof-of-concept study using a water-soluble phosphate salt prodrug of niclosamide[6], validating the well-accepted hypothesis [15] that improving water solubility and consequent oral bioavailability is critical in enabling niclosamide to reach solid tumors to exert its multi-faceted mechanisms. The phosphate salt approach is well established [16] and therefore lacks intellectual property potential; additionally, it caused a rapid spike in free niclosamide in the plasma, followed by rapid clearance, suggesting the need for frequent dosing and the potential for acute tissue toxicity with the sudden spike of niclosamide in tissues. Hoelzen et al

developed a valine niclosamide prodrug with enhanced water solubility and oral bioavailability; however, it lacked activity in a hollow fiber assay of HCC cell line[17]. A stearate prodrug nanoparticle platform for niclosamide was also shown to enhance bioavailability after IV injection (not oral administration) for the treatment of osteosarcoma [18, 19]. Given the limitations in the investigational niclosamide prodrugs, we aimed to design and develop novel niclosamide prodrugs, which can enhance oral bioavailability, sustain longer systemic exposure, while preserving its previously validated antitumor mechanisms. We evaluated the lead compound, SSL-0024, for its pharmacokinetic profile, safety, and anti-tumor efficacy in orthotopic HCC patient-derived xenograft (PDX) models, and confirmed its biological mechanisms of action.

Materials and Methods

Design, synthesis, and physicochemical characterization of novel niclosamide prodrug candidates

Based on existing patents and structure activity relationship studies of niclosamide[20], we designed over 50 novel potential prodrugs of niclosamide by modifying the 2-hydorxyl position with various sulfate and ester moieties. Of these, eight were initially synthesized by O2h Discovery (Cambridge, UK and India) (Table S1). Chemical structures were confirmed by ^{1}H-NMR spectroscopy, and purity determined by LC-MS/HPLC analysis. Detailed synthetic procedures and chemical analyses are provided in the Supplementary Materials.

All eight prodrug candidates were assayed for their kinetic and thermodynamic water solubility, pH stability (at 2.0 and 7.4), and in human plasma using standard assay protocols by O2h

Discovery (Cambridge, India); protocols are provided in the Supplementary Materials. Niclosamide (cat# N3510-50G, Millipore) and NEN (cat# 2A-9011637, 2A Biotech) were used as reference controls.

Culture of HCC cell lines

Human hepatocellular carcinoma (HCC) cell lines HepG2 (ATCC® HB-8065™, RRID: CVCL_0027) and Hep3B (ATCC® HB-8064™, RRID: CVCL_0326) were obtained from the American Type Culture Collection (ATCC), whereas Huh7 cells (JCRB0403, RRID: CVCL_0336) were provided by Dr. Mark Kay (Stanford University). HepG2 and Hep3B cells were cultured in Eagle's Minimum Essential Medium (EMEM; ATCC, cat# 30-2003), and Huh7 cells were maintained in Dulbecco's Modified Eagle's Medium (DMEM; ATCC, cat# 30-2002). All media were supplemented with 10% fetal bovine serum (FBS), 100 U/mL penicillin, and 100 µg/mL streptomycin (Life Technologies). Cells were maintained at 37°C in a humidified incubator with 5% CO_2.

Cell proliferation assay

The anti-proliferative effects of niclosamide prodrug candidates and niclosamide ethanolamine (used as a positive control) were assessed in HepG2, Huh7, and Hep3B cells using the CellTiter 96® Aqueous One Solution Cell Proliferation assay (MTS; Promega, cat# G4100). Cells were seeded into 96-well plates at a density of 3×10^3 cells per well and allowed to adhere overnight. A concentration range of 0.033–50 µM was used for each compound, over an incubation period of 72 hours. Following treatment, 15 µL of 3-(4,5-dimethylthiazol-2-yl)-5-(3-carboxymethoxyphenyl)-2-(4-sulfophenyl)-2H-tetrazolium, inner salt (MTS) reagent was added

to each well and incubated for 4 hours at room temperature. The resulting formazan product was solubilized by adding 100 µL of Stop Solution per well and incubating at 37°C for 1 hour before absorbance at 570 nm was measured using a SYNERGY-LX microplate reader (BioTek). Dose–response curves and half-maximal inhibitory concentration (IC_{50}) values were determined by nonlinear regression analysis using GraphPad Prism 11.0 (GraphPad Software, RRID:SCR_002798).

Pharmacokinetic and Tissue Distribution Analysis in Orthotopic Patient-Derived Xenograft model of HCC

All animal experiments were conducted in accordance with ARRIVE guidelines and approved by the Stanford University Institutional Animal Care and Use Committee (IACUC; Protocol APLAC-20167), complying with the USDA Animal Welfare Act, PHS Policy, and AAALAC International standards. Tumor size was monitored using calipers and did not exceed the maximum allowable diameter of 1.70 cm, with total tumor volume (calculated as $W^2 \times L/2$) not exceeding 10% of pre-inoculation body weight. Human HCC tissues were obtained from patients undergoing liver resection under an Institutional Review Board–approved protocol with informed consent. 6 to 10-week old male NOD-scid IL2Rgamma^{null} mice (NSG mice, Transgenic, Knockout and Tumor Model Center, Stanford University) were housed under controlled environmental conditions (12-h light/dark cycle, 20–24°C, 40–60% humidity) with ad libitum access to food and water.

To provide clinically relevant assessment of tumor and liver tissue exposure to niclosamide following administration of our prodrug candidates, we used an orthotopic HCC patient-derived

xenograft model, established using previously reported procedures[6]. Briefly, tumor fragments derived from resected patient samples were labeled with the luciferase reported gene and surgically implanted into the livers of NSG mice after initial subcutaneous engraftment on the shoulders of NSG mice. Tumor formation was monitored by bioluminescence imaging following injection of luciferin substrate (150 mg/kg) and monitored by Lago-X (Spectral Instruments Imaging).

Following confirmed tumor engraftment, PDX-bearing mice were given a single dose of SSL-0024 (50 mg/kg) or niclosamide (40 mg/kg). At predetermined time points (5 minutes, 30 minutes, 1, 4, 8, 24, and 48 hours post-administration), animals were anesthetized with isoflurane, and serial blood samples (50 µL each) were collected via saphenous vein (thigh) puncture. Blood samples were immediately transferred into EDTA-coated microtubes, centrifuged to obtain plasma, and stored at −80°C until further analysis. Since SSL-0024 was expected to release free niclosamide in vivo; we assessed the levels of niclosamide in the plasma and harvested livers and PDX tissues using a validated LC–MS/MS method performed by Medicilon (Boston).

In vivo efficacy study in orthotopic PDX HCC models

Following the procedure described above, PDX-bearing mice were randomized into three treatment groups (n=10 per group): vehicle control, SSL-0024 (100 mg/kg; molecular weight equivalent to 77.13 mg of niclosamide), or NEN (200 mg/kg, molecular weight equivalent to 168.57 mg of niclosamide). Compounds were administered once daily by oral gavage for 25 days.

Tumor progression was monitored weekly by bioluminescence imaging, and body weight was recorded three times per week. At study termination, PDX and adjacent liver tissues were harvested for niclosamide quantification by LC-MS/MS analysis (Medicilon, Boston) and immunohistochemical analysis. Blood was collected for analysis to determine effects on blood biochemistry, liver and kidney functions, and lipid metabolism at termination point (Stanford Animal Pathology Service).

Perioperative analgesia included Ethiqa-XR (3.25 mg/kg) administered prior to surgery, followed by postoperative Carprofen (10–25 mg/kg) as needed. Animals were monitored regularly for tumor burden and general health. Humane endpoints were applied in accordance with IACUC and AVMA guidelines. Euthanasia was performed by CO_2 inhalation or isoflurane anesthesia followed by cervical dislocation.

Tumor volume was quantified using standard volumetric calculations using the formula below:

$$\text{Tumor Volume}(\text{mm}^3) = \frac{\pi}{6} \times \text{Length}(\text{mm}) \times \text{Width}(\text{mm})^2$$

Immunohistochemistry

Formalin-fixed, paraffin-embedded tissue sections were deparaffinized in xylene and rehydrated through graded ethanol solutions to water. Antigen retrieval was performed using citrate buffer (cat# k035, Diagnostic Biosystems) under heat-mediated conditions, followed by cooling to room temperature. Endogenous peroxidase activity was quenched using blocking buffer, and sections were washed with phosphate-buffered saline (PBS).

Immunostaining was done for the proliferation marker Ki-67 and the apoptotic marker cleaved caspase-3, following manufacturer's instructions for primary monoclonal antibody against Ki-67 (1:20 dilution) (MA5-14520, Invitrogen™, Waltham), and polyclonal antibodies against caspase-

3 (1:300 dilution) (700182, Invitrogen). Briefly, slides were incubated with primary antibodies overnight at 4°C, followed by incubation with horseradish peroxidase (HRP)-conjugated secondary antibodies. Immunoreactivity was visualized using 3,3′-diaminobenzidine (DAB) substrate, and nuclei were counterstained with hematoxylin. After dehydration through graded ethanol and clearing in xylene, slides were mounted for microscopic evaluation.

Protein extraction and Western blotting

To assess the effects of niclosamide prodrug candidates on multiple signaling pathways, we treated Huh7 cells with 10x of IC_{50} dose of SSL-0024 for 24 hours, and protein levels were determined Western blotting.

Total protein was extracted from treated cells using T-PER Tissue Protein Extraction Reagent (Pierce, cat# 78510) and quantified by BCA Protein Assay (Pierce, cat# 23225). Equal amounts of protein (20 µg) were resolved on 4–12% polyacrylamide gels (Invitrogen) and transferred to polyvinylidene difluoride (PVDF) membranes. Membranes were blocked in 5% nonfat milk in TBST for 1 hour at room temperature and incubated overnight at 4°C with primary antibodies against LRP6 (Cell Signaling Technology, cat# 2560, RRID: AB_2139329, 1:1000 dilution), β-catenin (Cell Signaling Technology, cat# 8480, RRID: AB_11127855, 1:1000 dilution), STAT3 (Cell Signaling Technology, cat# 4904, RRID: AB_331269, 1:1000 dilution), phospho-STAT3 (Tyr705) (Cell Signaling Technology, cat# 9145, RRID: AB_2491009, 1:1000 dilution), Bcl-2 (Cell Signaling Technology, cat# 2870, RRID: AB_2290373, 1:1000 dilution), BCL-XL (Cell Signaling Technology, cat# 2764, RRID: AB_2228008, 1:1000 dilution), Cyclin D1 (Cell Signaling Technology, cat# 55506, RRID: AB_2827374, 1:1000 dilution), AKT (Cell Signaling Technology, cat# 9272S, RRID: AB_329827, 1:1000 dilution), phospho-AKT

(Ser473) (Cell Signaling Technology, cat# 9271S, RRID: AB_329825, 1:1000 dilution), mTOR (Cell Signaling Technology, cat# 2972, RRID: AB_2105622, 1:1000 dilution), phospho-mTOR (Ser2448) (Cell Signaling Technology, cat# 2971, RRID: AB_10691552, 1:1000 dilution), phospho-p70 S6 Kinase (Thr389) (Cell Signaling Technology, cat# 9234, RRID: AB_2269803, 1:1000 dilution), phospho-4EBP1 (Thr37/46) (Cell Signaling Technology, cat# 2855, RRID: AB_560835, 1:1000 dilution), EGFR (Cell Signaling Technology, cat# 2234, RRID: AB_331701, 1:1000 dilution), A-Raf (Cell Signaling Technology, cat# 2752, RRID: AB_330813, 1:1000 dilution), B-Raf (Cell Signaling Technology, cat# 9433, RRID: AB_2259354, 1:1000 dilution), phospho-B-Raf (Ser445) (Cell Signaling Technology, cat# 2696, RRID: AB_390721, 1:1000 dilution), C-Raf (Cell Signaling Technology, cat# 9422, RRID: AB_390808, 1:1000 dilution), phospho-C-Raf (Ser338) (Cell Signaling Technology, cat# 9427, RRID: AB_2067317, 1:1000 dilution), Vasorin (Abcam, cat# ab156868, 1:500 dilution), PD-L1 (Cell Signaling Technology, cat#13684, RRID: AB_2687655, 1:1000 dilution), ADAM17 (ABclonal, cat# A0821, RRID: AB_2757412, 1:1000 dilution), and GAPDH (Proteintech, cat# 60004-1-Ig, RRID: AB_2107436, 1:20,000 dilution).

After washing, membranes were incubated with fluorescent secondary antibodies (LI-COR Biosciences, IRDYE 800CW goat anti-rabbit, cat# 926-32211, RRID: AB_621843, 1:20,000 dilution; IRDYE 680RD goat anti-mouse, cat# 926-68070, RRID: AB_10956588, 1:20,000 dilution) at room temperature for 1 hour. Signals were detected and recorded using an Odyssey imaging system (LI-COR Biosciences) according to the manufacturer's instructions.

Statistical analysis

Data are presented as mean ± standard error of the mean (SEM). Statistical analyses were performed using GraphPad Prism software 11.0 (GraphPad Software, RRID:SCR_002798). For comparisons among multiple groups, one-way analysis of variance (ANOVA) was applied, followed by Tukey's post-hoc test when overall significance was achieved and variance homogeneity assumptions were satisfied.

To reduce interexperimental variability, data were normalized to matched baseline or vehicle control values (expressed as fold change or percentage of control) where appropriate. Parametric analyses were conducted only after verification of normality using the Shapiro–Wilk test ($\alpha = 0.05$) in conjunction with Q–Q plot assessment. For non-Gaussian distributions, log transformation was applied when it improved normality; if assumptions remained violated, nonparametric tests (e.g., Mann–Whitney U test) were used. Nonparametric approaches were also employed when normalized datasets exhibited zero variance within a reference group (e.g., control SEM = 0). A two-tailed P value < 0.05 was considered statistically significant.

Results

Physicochemical and in vitro activity profiling and lead prodrug selection

To overcome the poor aqueous solubility and limited bioavailability of niclosamide, we designed and synthesized eight structurally modified niclosamide prodrug candidates (Table S1; >95% chemical purity). These candidates were systematically evaluated for kinetic and thermodynamic solubility, chemical stability, plasma stability, and in vitro antiproliferative activity to identify

lead compound(s) suitable for in vivo development (Table 1). Niclosamide and NEN were used as reference controls for these evaluations.

SSL-0024 was the only candidate out of the tested eight that showed significant enhancements in kinetic (2.2-fold increase) and thermodynamic (5-fold increase) solubility compared to niclosamide. Additionally, SSL-0024 demonstrated high chemical stability under both physiological (pH 7.4) and gastric (pH 2.0) conditions, with minimal conversion to the parent compound over a 2-hour incubation period. In human plasma, 85.6% of SSL-0024 remained intact, indicating limited premature hydrolysis and suggesting the potential for controlled systemic release. Importantly, SSL-0024 retained anti-proliferative activity across three HCC cell lines (mean IC_{50} = 3.87 μM), confirming preservation of biological activity following structural modification of niclosamide.

All other prodrug candidates either lacked enhancements in water solubility (SSL-0048 to 0061), were unstable (SSL-0048 to 0061), or failed to show anti-proliferative effects in HCC cell lines (SSL-0048, 0049, 0050, 0058).

Collectively, these data identified SSL-0024 as the lead prodrug candidate for further pharmacokinetic and in vivo efficacy evaluation based on its favorable solubility, stability, and biological activity profiles.

Table 1 Physicochemical properties and in vitro potency of niclosamide prodrug candidates

Compound	Kinetic solubility	Thermodynamic solubility		pH7.4 (2h)		pH2.0 (2 h)		Human Plasma (2 h)		IC50 (μM)
	μM	μM	Equivalent conc. in μg/mL	% Remaining	% Niclosamide	% Remaining	% Niclosamide	% Remaining	% Niclosamide	(Average in 3 cell lines)
SSL-0024	**15**	**2**	**1**	**88**	**0**	**94**	**1.1**	**85.6**	**0.1**	**3.87**

SSL-0048	0.5	1	0	21.8	12.7	11.4	2.4	93.4	0.3	NA
SSL-0049	0.1	0.60	0.2	29.8	0.7	22.8	0.6	75.9	18.3	NA
SSL-0050	0.4	0.7	0.3	64.9	21.5	2.1	0.7	91.9	0.8	NA
SSL-0052	**3**	**3.0**	**1.3**	**76.2**	**22.3**	**37.4**	**32**	**0**	**71.9**	**2.51**
SSL-0053	**0.3**	**0.2**	**0.1**	**0**	**77.8**	**23.7**	**41.6**	**0**	**68.8**	**2.6**
SSL-0058	1.3	3.8	1.7	36	57.9	13.4	39.5	92.8	1.1	NA
SSL-0061	0.6	0.4	0.2	54.50	30.80	9.40	6.30	0.0	59.4	1.445
Niclosamide	6.9	0.5	0.2	85.2	NA	9.6	NA	96.8	NA	1.02
NEN	2.7	3.6	1.4	105.3	NA	11.9	NA	83.2	NA	1.03

Kinetic and thermodynamic solubility were measured under standardized assay conditions. Chemical stability and conversion to niclosamide were assessed following 2-hour incubation at pH 7.4, pH 2.0, and in human plasma. Percent remaining indicates intact prodrug, and percent niclosamide reflects conversion to the parent compound. IC_{50} values represent average antiproliferative activity across three cancer cell lines. Niclosamide and NEN were included as reference controls based on prior reports. NA: not available.

SSL-0024 Exhibits Extended Pharmacokinetics and Favorable Tissue Distribution

Plasma concentration–time profiling revealed a marked extension of systemic exposure for SSL-0024 when administered as a single oral dose of at 50 mg/kg to NSG mice bearing orthotopic HCC PDX. Specifically, SSL-0024 maintained detectable plasma levels beyond 24 hours (Fig. 1A). Niclosamide reached maximal plasma concentrations at 5 minutes (Tmax = 5 min), followed by a rapid elimination phase characterized by a sharp decline in systemic exposure; the same PK profile was observed with our proof-of-concept niclosamide phosphate salt prodrug [6]. Additionally, area under the plasma concentration–time curve from 0–24 h ($AUC_{0–24}h$) showed that SSL-0024 exhibited 6.6 times greater exposure than niclosamide within the shared 24-h

observation window (Fig. 1B), demonstrating greatly enhanced oral bioavailability compared to niclosamide.

After 24 or 48 hours, we sacrificed the mice and harvested liver and PDX tissues to assess the amount of free niclosamide released from SSL-0024; tissue distribution analysis revealed marked differences in niclosamide exposure between liver and PDX tumors. At 24 hours following SSL-0024 administration, liver niclosamide concentrations were substantially higher compared with that in PDX tissue (332.6 vs 91.4 ng/g). By contrast, at 48 hours, niclosamide levels had preferentially accumulated in PDX tumors compared to liver (66.8 vs 31 ng/g) (Fig. 1C). In comparison, niclosamide treatment resulted in consistently higher niclosamide accumulation in liver than in PDX tumors at the indicated time points (Fig. 1C). The remaining candidates exhibited limited tissue exposures (Fig. S2). These findings suggest that SSL-0024 provides substantially improved pharmacokinetic profile, with sustained plasma and tissue exposures.

Collectively, these results demonstrate that SSL-0024 achieves prolonged systemic exposure, enhanced overall drug exposure (significantly increased AUC), and favorable in vivo conversion to niclosamide. These pharmacokinetic advantages support its selection as a lead candidate for subsequent efficacy evaluation in orthotopic HCC models.

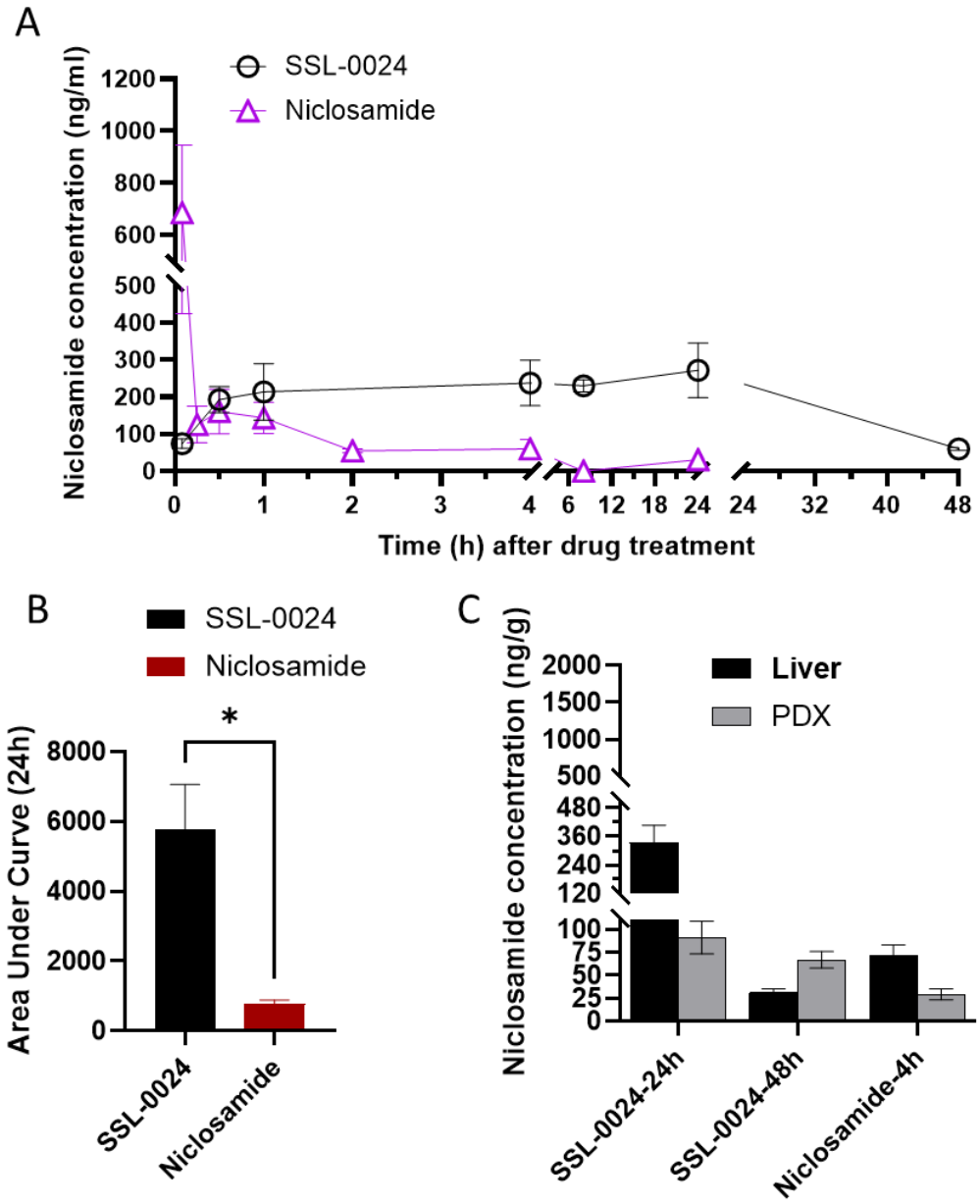

Figure 1. Pharmacokinetic and tissue distribution analysis of Niclosamide prodrugs.

(A) Plasma concentration–time profiles of SSL-0024 and niclosamide following oral administration (formulated in 0.5% methylcellulose).

(B) Area under the plasma concentration–time curve from 0–24 h ($AUC_{0–24}h$). SSL-0024 exhibited 6.56 times greater exposure than niclosamide within the shared 24-h observation window.

(C) Quantification of regenerated niclosamide levels in liver and orthotopic PDX tumor tissues following prodrug administration.

Plasma and tissue concentrations were quantified by LC-MS/MS. Data are presented as mean ± SEM, *$p < 0.05$ vs. control.

SSL-0024 Suppresses *in vivo* Growth of Orthotopic Patient-derived Xenograft of HCC

For the in vivo efficacy study, PDX-bearing mice were treated with either 100 mg/kg SSL-0024 (molecular weight equivalent to 77.13 mg of niclosamide) or 200 mg/kg NEN (molecular weight equivalent to 168.57 mg of niclosamide) via once-daily oral gavage for four weeks. NEN was used as the reference control rather than niclosamide, since we had shown earlier that niclosamide lacked in vivo activity [5]. The 100 mg/kg dose of SSL-0024 was selected based on our prior study with the niclosamide phosphate salt prodrug [6], which demonstrated strong tumor inhibition at a comparable molecular equivalent. SSL-0024 reduced tumor volume by 59.5% relative to control, whereas NEN reduced tumor volume by 43.7% (Fig. 2A–B). Although the difference between SSL-0024 and NEN was not statistically significant, SSL-0024 showed a trend toward greater tumor growth inhibition. Notably, this effect was achieved with a lower molecular weight equivalent of niclosamide (~45.8% of that in the NEN group).

Analysis of niclosamide concentrations in PDX tumors and livers revealed significantly higher drug accumulation with SSL-0024 compared to NEN (Fig. 2C). While NEN-treated mice exhibited ~1.7-fold higher niclosamide levels in normal adjacent liver versus PDX tissue, SSL-0024-treated mice showed ~1.2-fold higher niclosamide levels in PDX tumors than in normal liver (Fig. 2C), indicating preferential tumor accumulation. Additionally, niclosamide level in normal liver after SSL-0024 administration was ~6-fold higher than achieved with NEN, further supporting its enhanced bioavailability and tissue distribution. We also assessed niclosamide

distribution in the lung tissues, to determine lung toxicity. Niclosamide exposure in the lung was markedly lower than in the liver, corresponding to 0.48 times of liver levels after SSL-0024 administration and 0.34 times after NEN treatment (Fig. 2C). At the molecular level, SSL-0024 exhibited stronger inhibition of Ki-67 expression than NEN, suggesting enhanced anti-proliferative activity, while both compounds induced comparable increases in cleaved caspase-3, indicating similar pro-apoptotic effects (Fig. 2D–E). Collectively, these results demonstrate that SSL-0024 not only improves bioavailability and tumor-targeted accumulation but also achieves potent tumor growth inhibition with a favorable safety profile, highlighting its strong translational potential.

Body weight measurements throughout the treatment period revealed no significant weight losses in the SSL-0024 treated group compared to control and NEN treated groups (Fig 2F), suggesting its overall safety. Previous reports have suggested that NEN at 200 mg/kg q.d. induces alveolar toxicity due to degradation products including ethanolamine[21]; consistently, we observed similar pathologic changes in the lungs induced by NEN, but not in SSL-0024 treated group (Fig. 2G). Biochemical analysis for blood parameters, liver and kidney functions, and lipid metabolism indicate that treatment with SSL-0024 significantly increased WBC, neutrophil counts, alkaline phosphatase, and altered lipid profiles (cholesterol, HDL, LDL) compared to control, without major changes in RBC parameters or the liver enzymes AST (ALT showed elevated levels with high variability but remained within the normal range). NEN treatment had modest effects on MCV, MCH, monocytes %, AST, and alkaline phosphatase. Both compounds maintained normal RBC morphology and overall hematologic homeostasis, indicating tolerable systemic effects at the tested dose (Table S2).

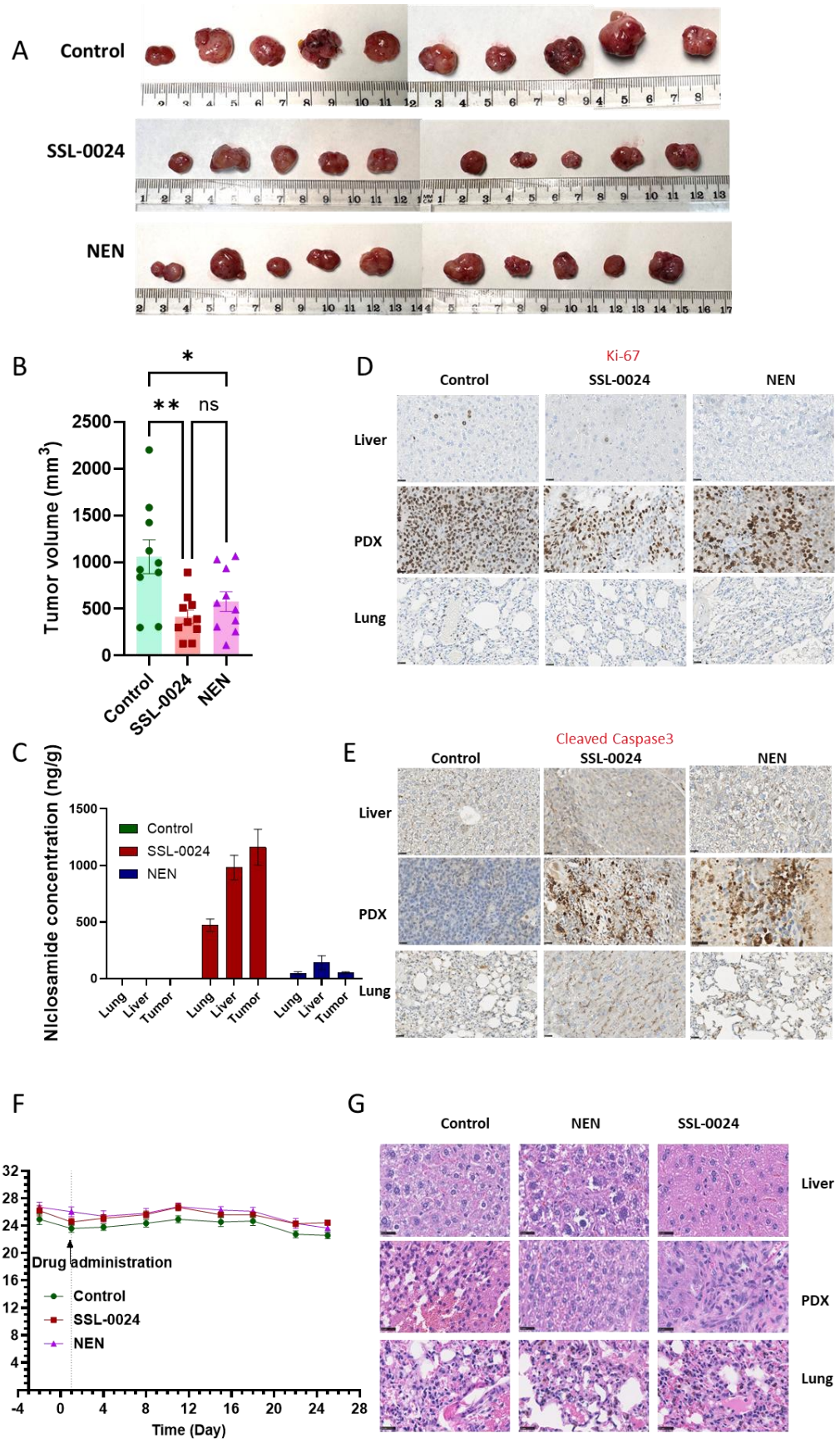
A
Control
SSL-0024
NEN
B
Tumor volume (mm3)
2500
2000
1500
1000
500
0
*
**
ns
Control
SSL-0024
NEN
C
NIclosamide concentration (ng/g)
1500
1000
500
0
Control
SSL-0024
NEN
Lung
Liver
Tumor
D
Ki-67
Control
SSL-0024
NEN
Liver
PDX
Lung
E
Cleaved Caspase3
Control
SSL-0024
NEN
Liver
PDX
Lung
F
Body weight (g)
32
28
24
20
16
12
8
4
Drug administration
Control
SSL-0024
NEN
-4
0
4
8
12
16
20
24
28
Time (Day)
G
Control
NEN
SSL-0024
Liver
PDX
Lung

Figure 2. SSL-0024 suppresses HCC PDX tumor growth and modulates proliferation and apoptosis markers.

A. Images of all harvested tumors collected at the end of the 25-days oral treatment period with SSL-0024 (100 mg/kg) or NEN (200 mg/kg).

B. Tumor volume measurements and statistical analysis over the 4-week treatment period (n = 10 per group). SSL-0024 reduced tumor volume by 59.5% compared to control, while NEN reduced tumor volume by 43.7%. Although the difference between SSL-0024 and NEN was not statistically significant, SSL-0024 showed a trend toward greater tumor inhibition.

C. Niclosamide concentrations in PDX tumor, liver, and lung tissues following treatment (n = 5 per group), quantified by LC-MS/MS. SSL-0024 achieved markedly higher accumulation in liver (981.79 vs. 142.97 ng/g) and tumor (1,161.89 vs. 53.89 ng/g) tissues compared to NEN, with preferential tumor distribution. Data are presented as mean ± SEM..

D–E. Immunohistochemical staining of Ki-67 (E) and cleaved caspase-3 (F) in PDX tumors. SSL-0024 demonstrated stronger inhibition of proliferation (Ki-67) and similar induction of apoptosis (cleaved caspase-3) relative to NEN, magnification: ×80.

(F) Body weight of tumor-bearing mice monitored throughout the 4-week treatment period. No significant body weight loss was observed across treatment groups, suggesting that SSL-0024 and NEN were well tolerated at the doses administered. Data are presented as mean ± SEM (n = 10).

(G) Representative hematoxylin and eosin (H&E) staining of liver, PDX tumor, and lung tissues. No obvious histopathological abnormalities were observed in liver or lung tissues following treatment, indicating acceptable systemic toxicity profiles for both SSL-0024 and NEN., magnification: ×80.

Data are presented as Mean ± SEM, *$p < 0.05$, **$p < 0.01$ vs. control

.

SSL-0024 regulates HCC growth *via* suppressing AKT–mTOR–STAT3, RAF, and Wnt signaling

To elucidate the mechanism underlying SSL-0024–mediated HCC growth inhibition, we focused on the AKT–mTOR–STAT3 signaling axis, a key pathway previously reported to be regulated by niclosamide [5]. Protein levels were normalized to control (set as 1), and relative changes were assessed for SSL-0024 and NEN groups.

SSL-0024 treatment significantly suppressed phosphorylation of critical signaling proteins, including p-STAT3 (Y705, 0.51), p-AKT (0.037), p-mTOR (0.28), p-4EBP1 (0.085), and p-p70S6K (0.18) (Fig. 3A-D,). Total STAT3 and total AKT were also significantly reduced by SSL-0024, whereas mTOR showed no statistically significant difference compared with control (Fig. 3C & 3D), indicating that SSL-0024 primarily inhibits the active, phosphorylated forms of these proteins. In contrast, NEN treatment led to a relatively modest reduction of STAT3, whereas BCL-XL was significantly decreased in the NEN group but remained unchanged in SSL-0024–treated tumors (Fig. 3A-D). Cyclin D1, a key downstream regulator of proliferation, was also significantly reduced by both SSL-0024 and NEN (Fig. 3A & 3B).

SSL-0024 treatment significantly reduced the expression of total A-Raf, total B-Raf and total C-Raf, and phosphorylated C-Raf, whereas phosphorylated B-Raf showed no statistically significant change (Fig. 3E–F; p-A-Raf could not be detected). These results indicate that SSL-0024 effectively suppresses RAF signaling, primarily through inhibition of C-Raf activation, a key driver of upstream MAPK signaling in HCC[22]. In contrast, NEN treatment showed no statistically significant changes in A-Raf, B-Raf, or phosphorylated B-Raf, while other proteins

including C-Raf, and phosphorylated C-Raf were significantly decreased. The expression of EGFR, which is an activator of both the AKT and RAS signaling cascades [23, 24], was significantly reduced by both SSL-0024 and NEN (Fig. 3C & 3D).

Two key components of the Wnt signaling pathway, LRP6 and β-catenin, were significantly down-regulated by both SSL-0024 and NEN (Fig. 3A & 3B).

Overall, these results demonstrate that SSL-0024 suppresses HCC growth through the inhibition of multiple crucial signaling pathways, and it achieves stronger inhibitory effects on most of the phosphorylated proteins compared with NEN, correlating with its enhanced in vivo anti-tumor effects.

Figure 3

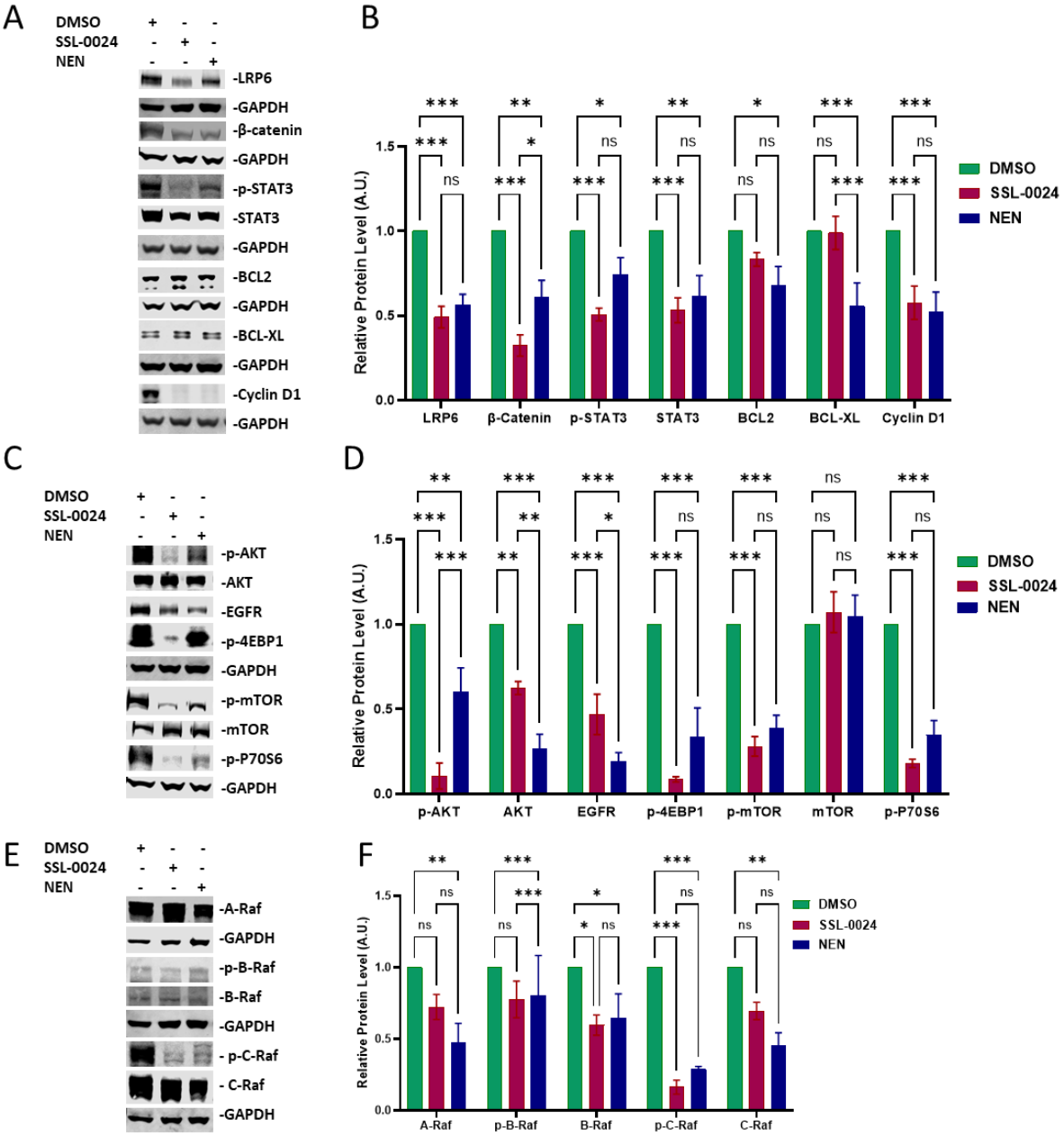
A
DMSO
SSL-0024
NEN
-LRP6
-GAPDH
-β-catenin
-GAPDH
-p-STAT3
-STAT3
-GAPDH
-BCL2
-GAPDH
-BCL-XL
-GAPDH
-Cyclin D1
-GAPDH
B
Relative Protein Level (A.U.)
LRP6
β-Catenin
p-STAT3
STAT3
BCL2
BCL-XL
Cyclin D1
DMSO
SSL-0024
NEN
C
-p-AKT
-AKT
-EGFR
-p-4EBP1
-GAPDH
-p-mTOR
-mTOR
-p-P70S6
-GAPDH
D
p-AKT
AKT
EGFR
p-4EBP1
p-mTOR
mTOR
p-P70S6
E
-A-Raf
-GAPDH
-p-B-Raf
-B-Raf
-GAPDH
- p-C-Raf
- C-Raf
-GAPDH
F
A-Raf
p-B-Raf
B-Raf
p-C-Raf
C-Raf

Fig. 3. SSL-0024 modulates multiple signaling pathways.

(A) Representative immunoblot analysis of LRP, β-catenin, p-STAT3 (Y705), total STAT3, BCL2, BCL-XL, and Cyclin D1 protein levels following SSL-0024 treatment. (B) Quantification of protein expression levels shown in (A).

(C) Representative immunoblot analysis of p-AKT, total AKT, EGFR, p-4EBP1, p-mTOR, total mTOR, and p-p70S6K following SSL-0024 treatment.

(D) Quantification of protein expression levels shown in (C).

(E) Representative immunoblot analysis of total A-Raf, p-B-Raf, total B-Raf, p-C-Raf, and total C-Raf following SSL-0024 treatment.

(F) Quantification of protein expression levels shown in (E).

Protein levels were quantified by densitometry and expressed as arbitrary units (A.U.). Phosphorylated proteins were normalized to their respective total protein levels, except p-4EBP1 which was normalized to GAPDH due to the unavailability of a reliable total 4EBP1 signal. All other total proteins were normalized to GAPDH. Data are presented as relative protein levels A.U. ± SEM. n = 3. *$p < 0.05$, **$p < 0.01$, ***$p < 0.001$ vs. control.

SSL-0024 regulates HCC growth *via* suppressing VASN and PD-L1 protein expression

Consistent with our previous study using niclosamide phosphate salt [5, 6], observed that SSL-0024 strongly inhibited VASN and PD-L1 expression (Fig. 4A & 4B). To assess the upstream regulation of VASN, we measured ADAM17, the metalloprotease responsible for VASN cleavage and subsequent activation of TGFβ signaling [25]. SSL-0024 treatment decreased ADAM17 levels (Fig. 4A & 4B), suggesting reduced VASN secretion and suppression of TGFβ-mediated pro-tumor signaling.

In addition to the validated changes in oncogenic signaling pathways, we showed that SSL-0024 additionally acts via the novel target VASN and its associated proteins, as well as PD-L1 (Fig. 4A & 4B), supporting its multi-targeted mechanism and superior anti-tumor potential.

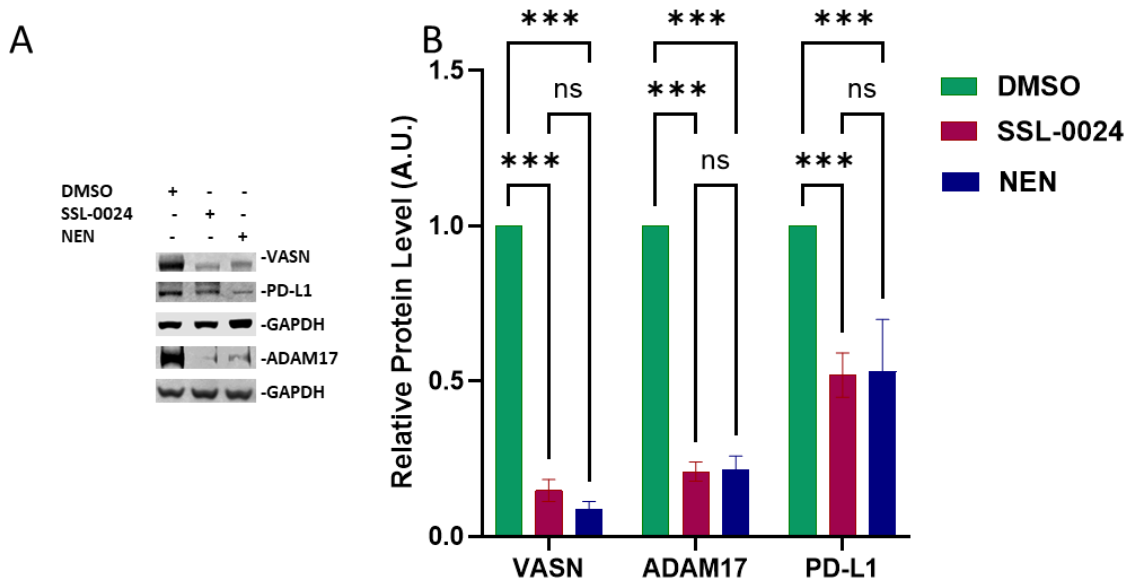

Fig.4. SSL-0024 regulates VASN-associated protein expression.

(A) Representative immunoblot analysis of VASN, PD-L1, and ADAM17 following SSL-0024 treatment. (H–J) Quantification of protein expression levels shown in (A).

Protein levels were quantified by densitometry and expressed as arbitrary units (A.U.). All proteins were normalized to GAPDH. Data are presented as relative protein levels A.U. ± SEM. n = 3. ***$p < 0.001$ vs. control.

Discussion

By rationally designing and systematically screening eight novel prodrug candidates of niclosamide, we identified a lead prodrug, SSL-0024 (niclosamide-O-sulfate ammonium salt), which showed favorable water solubility, pH stability, improved PK profile/oral bioavailability, and in vitro and in vivo anti-tumor efficacy. In particular, SSL-0024 achieves sustained systemic exposure beyond 24 hours after a single dose, whereas native niclosamide exhibits a plasma half-life averaging 4 to 5 hours [26]. This prolonged half-life enhances bioavailability so that there is a steady level of active parent drug reaching the tumors; consequently, we observed effective tumor suppression at only ~45.8% of the dose required for NEN, without detectable systemic toxicity. By reducing the dosing requirement while maintaining efficacy, SSL-0024 demonstrates a substantially improved therapeutic index, supporting once-daily oral administration and highlighting its potential for clinical use in HCC patients. This pharmacokinetic improvement directly addresses the historical barrier that has limited niclosamide clinical translation and potentially enables sustained inhibition of multiple oncogenic pathways critical for HCC growth and survival.

Aryl sulfatases in liver cells[27] are expected to cleave SSL-0024 to release free niclosamde. We observed stability of our sulfate ammonium salt prodrug under gastric and plasma pH conditions, a steady release of free niclosamide into plasma over the 48 hours period, as well as accumulation of free niclosamide in the liver and PDX tissues. The ammonium sulfate counterion that is also released upon cleavage is labeled by the Food and Drug Administration as being “Generally Recognized As Safe” (GRAS), and is a commonly used food additive safe for general human consumption. Having a safe counterion is an important criterion in the selection of counterions in prodrug design[28, 29] , and is what we have achieved in this study. In contrast, NEN dissociates into free niclosamide and ethanolamine, which is a known lung irritant [30], likely

responsible for the pathologic changes in lung alveolar that we observed upon NEN treatment. The lung toxicity observed upon NEN administration was absent with SSL-0024 treatment. Therefore, SSL-0024 is more efficacious and less toxic than NEN, which has not been approved by the FDA for human use.

Mechanistically, we confirmed that SSL-0024 suppresses a convergent oncogenic signaling network central to HCC progression, aligned with the reported actions of its parent drug, niclosamide. We observed coordinated inhibition of the mTOR–AKT–STAT3 axis, evidenced by reduced phosphorylation of AKT, mTOR, 4EBP1, p70S6K, and STAT3 (Y705), together with downregulation of Cyclin D1, BCL2, and BCL-XL. Concurrent attenuation of RAF isoforms suggests disruption of growth factor–driven mitogenic signaling [31]. By simultaneously inhibiting mTOR–AKT–STAT3 and RAF–MEK–ERK cascades, SSL-0024 may prevent compensatory signaling that often drives resistance to monotherapies. This network-level suppression is clinically relevant, as multi-kinase inhibitors such as Sorafenib rely on similar pathways, and resistance frequently arises via adaptive PI3K–AKT or RAF–MEK–ERK activation [32-35]. Sustained STAT3 inhibition is particularly important given its established role in promoting proliferation, survival, and immune evasion in liver cancer [36-38]. Simultaneous multi-pathway inhibition may limit adaptive resistance often observed with single-target therapies, providing a rationale for more durable tumor control in HCC [39].

SSL-0024 reduced LRP6 expression to a degree comparable to NEN; however, β-catenin suppression was notably more pronounced following SSL-0024 treatment. Since β-catenin is a key downstream effector of LRP6-mediated Wnt signaling and drives transcription of proliferation-associated genes[40], the disproportionate reduction in β-catenin suggests that SSL-0024 may modulate β-catenin stability or activity through mechanisms beyond receptor-level

suppression. These findings suggest that enhanced attenuation of canonical Wnt/β-catenin signaling may contribute, at least in part, to the superior anti-proliferative effects of SSL-0024. In our prior study on niclosamide phosphate salt prodrug [6], VASN knockdown phenocopied drug treatment, and VASN rescue attenuated antitumor effects, establishing VASN as a functional mediator of niclosamide-derived activity. Consistent with this mechanism, SSL-0024 similarly reduced VASN expression, presumable via the release of free niclosamide. Together, these findings indicate that SSL-0024 conserves the previously validated VASN-dependent signaling axis, and that our rational structural modification does not compromise mechanistic targeting, reinforcing confidence in its antitumor activity.

Beyond tumor-intrinsic signaling, SSL-0024 reduced PD-L1 expression, a central mediator of immune escape in HCC and a clinically actionable target [41]. Although the precise regulatory mechanism underlying PD-L1 downregulation by SSL-0024 remains to be determined, one possible contributing mechanism might be the suppression of STAT3 signaling, a well-known transcriptional regulator of PD-L1 in multiple cancers, for instance lung cancer, natural killer/T-cell lymphoma, breast cancer, head and neck squamous cell carcinoma, and HCC[42-48] . This dual inhibition of proliferative and immune-evasive pathways suggests that SSL-0024 could provide additive or synergistic effects when combined with immune checkpoint inhibitors. Future studies should evaluate SSL-0024 in combination with immune checkpoint inhibitors or kinase inhibitors for potential synergistic efficacy. Its ability to modulate both tumor growth and immune evasion highlights the potential for rational combination strategies with current standard-of-care therapies.

From a translational perspective, SSL-0024 offers the additional advantage of a simple one-step synthesis from readily available chemical precursors, facilitating scalable production and

potentially reducing cost. Compared with current therapies, including Sorafenib, Lenvatinib, or checkpoint inhibitors such as Atezolizumab, SSL-0024 combines multi-pathway tumor suppression with potential immune modulation in a single orally available agent. Together with prolonged systemic exposure, reduced effective dosing, and minimal toxicity, these attributes position SSL-0024 as a pharmacologically optimized derivative with improved drug-like properties relative to earlier niclosamide formulations.

Several limitations of this study warrant consideration. First, although SSL-0024 was observed to suppress key signaling pathways, formal pharmacokinetic–pharmacodynamic correlation analyses were not performed, which would strengthen mechanistic linkage between systemic exposure and target inhibition. Second, while PD-L1 reduction was observed, comprehensive characterization of the tumor immune microenvironment and assessment of immune cell infiltration were beyond the scope of this study. Third, combination efficacy with approved HCC therapies, including Sorafenib, Lenvatinib, or immune checkpoint inhibitors, remains to be evaluated. Fourth, dose-escalation studies to define the maximum tolerated dose and therapeutic window, particularly in orthotopic PDX models, would provide valuable translational insight. Finally, additional investigation into other potentially relevant signaling networks, such as insulin-like growth factor regulation, may identify further opportunities for therapeutic synergy.

Conclusion

In summary, SSL-0024 exemplifies how rational prodrug optimization can transform a biologically validated but clinically impractical compound into a therapeutically viable drug candidate for solid tumors. The enhanced and sustained systemic exposure, together with coordinated oncogenic pathway suppression, suggests the promising potential of SSL-0024 as a readily translatable niclosamide prodrug for HCC therapy. Our findings lay a strong foundation

for further mechanistic exploration, combination therapy studies, and translational development toward clinical application, offering a compelling path forward for niclosamide-based therapeutic strategies in HCC.

List of abbreviations

Abbreviation	Full name
^{1}H-NMR	Proton nuclear magnetic resonance
ANOVA	Analysis of variance
AUC	Area under curve
DAB	3,3′-diaminobenzidine
FBS	Fetal bovine serum
GRAS	Generally recognized as safe
HCC	Hepatocellular carcinoma
HPLC	High-performance liquid chromatography
HRP	Horseradish peroxidase
IACUC	Institutional Animal Care and Use Committee
IC_{50}	Half-maximal inhibitory concentration
LC-MS	Liquid chromatography-mass spectrometry
MTS	3-(4,5-dimethylthiazol-2-yl)-5-(3-carboxymethoxyphenyl)-2-(4-sulfophenyl)-2H-tetrazolium, inner salt
NEN	Niclosamide ethanolamine
NSG	NOD scid gamma
PDX	Patient-derived xenografts
PVDF	Polyvinylidene difluoride
SEM	Standard error of the mean

Acknowledgement

We are grateful to the Stanford Cell Sciences Imaging Facility for providing training and usage support with RRID:SCR_017787.

AUTHOR CONTRIBUTIONS

Conceived study: Mei-Sze Chua, Steve Schow, Robert Lum, Samuel So. Design of compounds: Steve Schow, Robert Lum. Designed experiments: Mingdian Tan, Mei-Sze Chua, Renumathy Dhanasekaran. Participated in/executed trial/study: Mingdian Tan, Yi Liu, Dawiyat Massoudi. Data collection/acquisition: Mingdian Tan, Yi Liu, Dawiyat Massoudi. Data analysis: Mingdian Tan, Mei-Sze Chua, Dawiyat Massoudi. Data interpretation: Mingdian Tan, Steve Schow, Mei-Sze Chua, Renumathy Dhanasekaran. Manuscript writing: Mingdian Tan, Mei-Sze Chua, Steve Schow. Supervision of study: Mei-Sze Chua, Renumathy Dhanasekaran, Samuel So. Approval of final submitted version: Mingdian Tan, Mei-Sze Chua, Steve Schow, Robert Lum, Yi Liu, Dawiyat Massoudi, Renumathy Dhanasekaran, and Samuel So.

Funding

This project was supported by the CJ Huang Foundation, and by Mavis and CH Fong, to M.S.C., M.T., and Y.L.

Data availability

The datasets used and/or analyzed during the current study are available from the corresponding author on reasonable request.

Ethics declarations

Ethics approval and consent to participate

All animal experiments were conducted in accordance with the ARRIVE guidelines and approved by the Stanford University Institutional Animal Care and Use Committee (IACUC; Protocol APLAC-20167), complying with the USDA Animal Welfare Act, PHS Policy, and AAALAC International standards. Tumor size was monitored using calipers and did not exceed

the maximum allowable diameter of 1.70 cm, with total tumor volume (calculated as $W^2 \times L/2$) not exceeding 10% of pre-inoculation body weight. Human HCC tissues were obtained from patients undergoing liver resection under an IRB-approved protocol (IRB #26562), and written informed consent was obtained from all participants prior to enrollment. No client-owned animals were used.

Consent for publication

All the authors have read and approved the final manuscript and consent to its publication.

Competing interests

The authors declare no competing interests.

References

1. Singh, S.P., Madke, T. & Chand, P. Global Epidemiology of Hepatocellular Carcinoma. *J Clin Exp Hepatol* **15**, 102446 (2025).
2. Amin, N., Anwar, J., Sulaiman, A., Naumova, N.N. & Anwar, N. Hepatocellular Carcinoma: A Comprehensive Review. *Diseases* **13** (2025).
3. Lu, W. *et al.* Niclosamide suppresses cancer cell growth by inducing Wnt co-receptor LRP6 degradation and inhibiting the Wnt/beta-catenin pathway. *PLoS One* **6**, e29290 (2011).
4. Wang, C. *et al.* Niclosamide Inhibits Cell Growth and Enhances Drug Sensitivity of Hepatocellular Carcinoma Cells via STAT3 Signaling Pathway. *J Cancer* **9**, 4150-4155 (2018).
5. Chen, B. *et al.* Computational Discovery of Niclosamide Ethanolamine, a Repurposed Drug Candidate That Reduces Growth of Hepatocellular Carcinoma Cells In Vitro and in Mice by Inhibiting Cell Division Cycle 37 Signaling. *Gastroenterology* **152**, 2022-2036 (2017).
6. Tan, M. *et al.* Niclosamide prodrug enhances oral bioavailability and efficacy against hepatocellular carcinoma by targeting vasorin-TGFbeta signalling. *Br J Pharmacol* **182**, 5517-5535 (2025).
7. Liu, Y. *et al.* Lipid-Based Self-Microemulsion of Niclosamide Achieved Enhanced Oral Delivery and Anti-Tumor Efficacy in Orthotopic Patient-Derived Xenograft of Hepatocellular Carcinoma in Mice. *Int J Nanomedicine* **19**, 2639-2653 (2024).

8. Qin, J.J., Yan, L., Zhang, J. & Zhang, W.D. STAT3 as a potential therapeutic target in triple negative breast cancer: a systematic review. *J Exp Clin Cancer Res* **38**, 195 (2019).
9. Sack, U. *et al.* Novel effect of antihelminthic Niclosamide on S100A4-mediated metastatic progression in colon cancer. *Journal of the National Cancer Institute* **103**, 1018-1036 (2011).
10. Liu, C. *et al.* Niclosamide inhibits androgen receptor variants expression and overcomes enzalutamide resistance in castration-resistant prostate cancer. *Clin Cancer Res* **20**, 3198-3210 (2014).
11. Kim, M.Y. *et al.* Niclosamide exerts anticancer effects through inhibition of the FOXM1-mediated DNA damage response in prostate cancer. *Am J Cancer Res* **11**, 2944-2959 (2021).
12. Kumar, R. *et al.* Mitochondrial uncoupling reveals a novel therapeutic opportunity for p53-defective cancers. *Nat Commun* **9**, 3931 (2018).
13. Yang, Z., Li, H., Yang, B. & Liu, Y. Albumin-Based Microneedles for Spatiotemporal Delivery of Temozolomide and Niclosamide to Resistant Glioblastoma. *ACS Appl Mater Interfaces* **16**, 44518-44527 (2024).
14. Satoh, K. *et al.* Identification of Niclosamide as a Novel Anticancer Agent for Adrenocortical Carcinoma. *Clin Cancer Res* **22**, 3458-3466 (2016).
15. Muller, C.E. Prodrug approaches for enhancing the bioavailability of drugs with low solubility. *Chem Biodivers* **6**, 2071-2083 (2009).
16. Tantra, T. *et al.* Phosphate Prodrugs: An Approach to Improve the Bioavailability of Clinically Approved Drugs. *Curr Med Chem* **31**, 336-357 (2024).
17. Hoelzen, E.J. *et al.* Valine-Niclosamide for Treatment of Androgen Receptor Splice Variant-Positive Hepatocellular Carcinoma. *Cancers* **17** (2025).
18. Reddy, G.B. *et al.* Preclinical Testing of a Novel Niclosamide Stearate Prodrug Therapeutic (NSPT) Shows Efficacy Against Osteosarcoma. *Mol Cancer Ther* **19**, 1448-1461 (2020).
19. Eward, W.C. *et al.* Novel niclosamide stearate prodrug therapeutic shows potential efficacy against naturally occurring canine osteosarcoma in a clinical feasibility study. *Am J Vet Res* **87** (2026).
20. Tang, Z. *et al.* Structure-Activity Relationship of Niclosamide Derivatives. *Anticancer Res* **37**, 2839-2843 (2017).
21. P, J. *et al.* Isolation, characterization using LC-ESI-QTOF, NMR and in vitro cytotoxicity assay of niclosamide forced degradation products. *J Pharm Biomed Anal* **136**, 148-155 (2017).
22. Riaud, M. *et al.* The role of CRAF in cancer progression: from molecular mechanisms to precision therapies. *Nat Rev Cancer* **24**, 105-122 (2024).
23. Wee, P. & Wang, Z. Epidermal Growth Factor Receptor Cell Proliferation Signaling Pathways. *Cancers* **9** (2017).
24. Levantini, E., Maroni, G., Del Re, M. & Tenen, D.G. EGFR signaling pathway as therapeutic target in human cancers. *Semin Cancer Biol* **85**, 253-275 (2022).
25. Malapeira, J., Esselens, C., Bech-Serra, J.J., Canals, F. & Arribas, J. ADAM17 (TACE) regulates TGFbeta signaling through the cleavage of vasorin. *Oncogene* **30**, 1912-1922 (2011).

26. Chen, W., Mook, R.A., Jr., Premont, R.T. & Wang, J. Niclosamide: Beyond an antihelminthic drug. *Cellular signalling* **41**, 89-96 (2018).
27. Van Berkel, T.J., Kruijt, J.K. & Koster, J.F. Identity and activities of lysosomal enzymes in parenchymal and non-parenchymal cells from rat liver. *Eur J Biochem* **58**, 145-152 (1975).
28. Gupta, D., Bhatia, D., Dave, V., Sutariya, V. & Varghese Gupta, S. Salts of Therapeutic Agents: Chemical, Physicochemical, and Biological Considerations. *Molecules* **23** (2018).
29. Gould, P.L. Salt selection for basic drugs. *International Journal of Pharmaceutics* **33**, 201-217 (1986).
30. Fiume, M.M. *et al.* Safety Assessment of Ethanolamine and Ethanolamine Salts as Used in Cosmetics. *Int J Toxicol* **34**, 84S-98S (2015).
31. Bahar, M.E., Kim, H.J. & Kim, D.R. Targeting the RAS/RAF/MAPK pathway for cancer therapy: from mechanism to clinical studies. *Signal Transduct Target Ther* **8**, 455 (2023).
32. Eun, J.W. *et al.* Cancer-associated fibroblast-derived secreted phosphoprotein 1 contributes to resistance of hepatocellular carcinoma to sorafenib and lenvatinib. *Cancer Commun (Lond)* **43**, 455-479 (2023).
33. Tang, W. *et al.* The mechanisms of sorafenib resistance in hepatocellular carcinoma: theoretical basis and therapeutic aspects. *Signal Transduct Target Ther* **5**, 87 (2020).
34. Wang, X. *et al.* Sorafenib combined with STAT3 knockdown triggers ER stress-induced HCC apoptosis and cGAS-STING-mediated anti-tumor immunity. *Cancer Lett* **547**, 215880 (2022).
35. Zhang, H., Wang, Q., Liu, J. & Cao, H. Inhibition of the PI3K/Akt signaling pathway reverses sorafenib-derived chemo-resistance in hepatocellular carcinoma. *Oncol Lett* **15**, 9377-9384 (2018).
36. Hu, B. *et al.* Inhibition of EGFR Overcomes Acquired Lenvatinib Resistance Driven by STAT3-ABCB1 Signaling in Hepatocellular Carcinoma. *Cancer Res* **82**, 3845-3857 (2022).
37. Liu, Y. *et al.* HERC2 promotes inflammation-driven cancer stemness and immune evasion in hepatocellular carcinoma by activating STAT3 pathway. *J Exp Clin Cancer Res* **42**, 38 (2023).
38. Hashemi, M. *et al.* Deciphering STAT3 signaling potential in hepatocellular carcinoma: tumorigenesis, treatment resistance, and pharmacological significance. *Cell Mol Biol Lett* **28**, 33 (2023).
39. Ladd, A.D., Duarte, S., Sahin, I. & Zarrinpar, A. Mechanisms of drug resistance in HCC. *Hepatology* **79**, 926-940 (2024).
40. Wu, X., Que, H., Li, Q. & Wei, X. Wnt/beta-catenin mediated signaling pathways in cancer: recent advances, and applications in cancer therapy. *Mol Cancer* **24**, 171 (2025).
41. Finn, R.S. *et al.* Atezolizumab plus Bevacizumab in Unresectable Hepatocellular Carcinoma. *The New England journal of medicine* **382**, 1894-1905 (2020).
42. Xie, C. *et al.* Apatinib triggers autophagic and apoptotic cell death via VEGFR2/STAT3/PD-L1 and ROS/Nrf2/p62 signaling in lung cancer. *J Exp Clin Cancer Res* **40**, 266 (2021).

43. Papavassiliou, K.A., Marinos, G. & Papavassiliou, A.G. Combining STAT3-Targeting Agents with Immune Checkpoint Inhibitors in NSCLC. *Cancers* **15** (2023).
44. Jeong, H. *et al.* Cell-intrinsic PD-L1 signaling drives immunosuppression by myeloid-derived suppressor cells through IL-6/Jak/Stat3 in PD-L1-high lung cancer. *J Immunother Cancer* **13** (2025).
45. Song, T.L. *et al.* Oncogenic activation of the STAT3 pathway drives PD-L1 expression in natural killer/T-cell lymphoma. *Blood* **132**, 1146-1158 (2018).
46. Zerdes, I. *et al.* STAT3 Activity Promotes Programmed-Death Ligand 1 Expression and Suppresses Immune Responses in Breast Cancer. *Cancers* **11** (2019).
47. Bu, L.L. *et al.* STAT3 Induces Immunosuppression by Upregulating PD-1/PD-L1 in HNSCC. *J Dent Res* **96**, 1027-1034 (2017).
48. Sukowati, C. *et al.* PD-L1 Downregulation and DNA Methylation Inhibition for Molecular Therapy against Cancer Stem Cells in Hepatocellular Carcinoma. *Int J Mol Sci* **24** (2023).

Problem

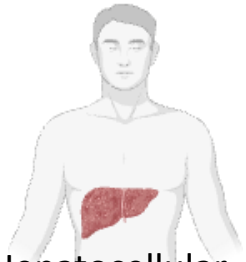

Hepatocellular carcinoma (HCC)

Native Niclosamide
Poor Aqueous Solubility

Low Oral Bioavailability

Short Systemic Exposure

Limits Sustained Tumor Suppression

Solution

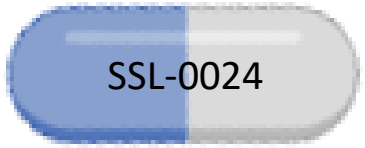

Niclosamide Prodrug

Improved PK For Oral Dosing

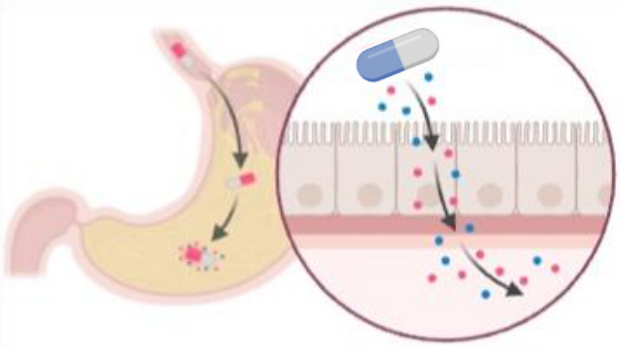

- Higher Aqueous Solubility
- Stable In Gastric & Plasma Conditions
- Enables Sustained Pharmacology in Vivo

Outcome

In Vivo Efficacy

Orthotopic HCC patient-derived xenograft Models

~60% Tumor Growth Inhibition

At ~46.8% Of Prior Control Dose
Niclosamide Ethanolamine Salt (NEN)

Multi-pathway Signaling Inhibition

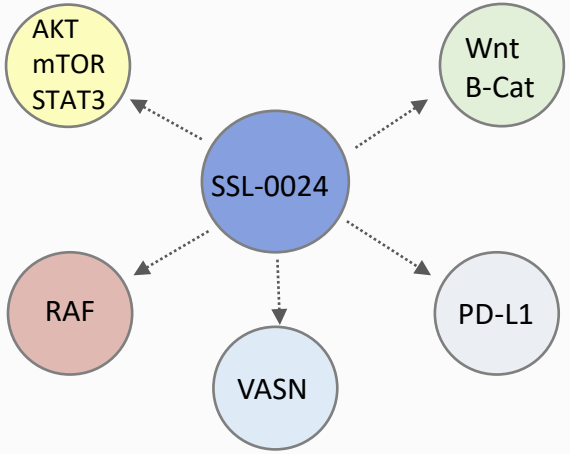

↓Proliferation • ↓Survival • ↓Immune Evasion